A highly effective in vivo photothermal nanoplatform with dual imaging-guided therapy of cancer based on the charge reversal complex of dye and iron oxide

Chang, Y.; Li, X.; Kong, X.; Li, Y.; Liu, X.; Zhang, Y.; Tu, L.; Xue, B.; Wu, F.; Cao, D.; Zhao, H.; Zhang, H.

DOI
10.1039/c5tb01455g

Publication date
2015

Document Version
Final published version

Published in
Journal of Materials Chemistry. B

License
Article 25fa Dutch Copyright Act

Journal of Materials Chemistry B

PAPER

View Article Online
View Journal | View Issue

Cite this: J. Mater. Chem. B, 2015, 3, 8321

A highly effective *in vivo* photothermal nanoplatform with dual imaging-guided therapy of cancer based on the charge reversal complex of dye and iron oxide†

Yulei Chang,[a] Xiaodan Li,[b] Xianggui Kong,[a] Ye Li,[b] Xiaomin Liu,*[a] Youlin Zhang,*[a] Langping Tu,[a] Bin Xue,[a] Fei Wu,[a] Dianbo Cao,[b] Huiying Zhao[b] and Hong Zhang*[c]

Received 21st July 2015,
Accepted 9th September 2015

DOI: 10.1039/c5tb01455g

www.rsc.org/MaterialsB

To enhance the treatment efficiency of photothermal therapy (PTT) with very little light-associated side effect, we have constructed a highly effective PTT nanoplatform for fluorescence and MRI dual imaging-guided PTT of cancer, based on IR806 dye and iron oxide complex functionalized with mPEG-PCL-G2.0PAMAM-Cit, which can be for charge-conversion for targeted accumulation in tumor. Combination of iron oxide nanoparticles and IR806 improve light to thermal conversion efficiency and lower light irradiation dose. *In vitro* and *in vivo* tests demonstrated that an effective dual imaging-guided PTT as low as 0.25 W cm^{-2} could be realized under a light irradiation of 808 nm. These efforts highlight the potential of this PTT nanoplatform in "precision medicine".

1 Introduction

Photothermal therapy (PTT) is a light-triggered non-invasive and effective modality for cancer treatment, which is based on rapid electron–phonon interaction with the aid of photothermal conversion agents that selectively tumors.[1–3] In the PTT, the photothermal agent absorbs the irradiation light and converts it into local hyperthermia, resulting in tumor cell death. This thermal ablation treatment notably improves selectivity and has lesser side effects compared to traditional radio-/chemo-therapies.[4,5] Nevertheless, the current PTT treatment of tumors has a number of deficiencies: the relatively high irradiation dose of light, the poor accurate therapy without a locating means and the lack of targeted accumulation in the tumor.[3,4,6] Moreover, the demands of precision medicine for the visualization of the specific accumulation, the intratumoral distribution and the kinetics of drug release of the agent are also very critical for an efficient therapy.[7–10] This status promotes the development of theranostic agents for targeting and/or imaging-guided PTT.

In recent years, a large number of PTT materials, including carbon-based materials,[11,12] noble metal materials,[13–15] organic[16–18] and inorganic materials,[14,19,20] have been explored as potential PTT agents. Among these, iron oxide nanoparticles (IONPs) have attracted great attention.[19,21–23] IONPs have excellent magnetic properties and are biocompatible and potentially non-toxic. They have been employed as carriers for drug delivery and as magnetic resonance imaging (MRI) contrast agents. Importantly, they are also a type of agents for NIR light-induced PTT by themselves. However, high irradiation density of light (over 1 W cm^{-2})[3,21,24] or high concentration of IONPs is generally required in PTT for effective ablation of the tumor.[24] In this respect, NIR dyes may play a constructive role because they have strong absorption in the "first optical biological window", which may facilitate the PTT efficacy and deep penetration of the light into the tissue. To date, they have been widely used as imaging agents[8,25,26] and photothermal agents.[8,16,27] Recently, although a few studies have reported a combination of NIR dyes and IONPs as dual imaging agents; the PTT effect of the coupling, in their opinion, was achieved mainly by molecular heat.[28]

Considering the advantages of NIR dyes and IONPs as photothermal agents, in this work, we constructed a highly effective PTT nanoplatform by anchoring IR806 on the surface of IONPs, greatly improving the light to thermal efficiency of the complex. Moreover, we synthesized a novel triple-copolymer of mPEG-PCL-G2.0-Cit to modify the IR806–IONPs complex, where citraconic anhydride (Cit) is introduced as a smart charge-conversion agent to improve the targeted accumulation in the tumor. Importantly, the PTT platform can also be used for fluorescence and MRI dual imaging-guided PTT. *In vitro* and *in vivo* tests are performed to validate the strategy.

[a] State Key Laboratory of Luminescence and Applications, Changchun Institute of Optics, Fine Mechanics and Physics, Chinese Academy of Sciences, Changchun 130033, China. E-mail: xmliu@ciomp.ac.cn, zhangyl@ciomp.ac.cn
[b] The First Hospital of Jilin University, Changchun 130021, China
[c] Van't Hoff Institute for Molecular Sciences, University of Amsterdam, Science Park 904, 1098 XH Amsterdam, The Netherlands. E-mail: h.zhang@uva.nl

† Electronic supplementary information (ESI) available. See DOI: 10.1039/c5tb01455g

2 Experimental and methods

2.1. Materials

IR780 iodide, methoxypolyethylene glycol (mPEG) ε-caprolactone (CL), 4-dimethylaminopyridine (DMAP), 4-mercaptobenzoic acid (4MBA), trypan blue, *N*-(3-dimethylaminopropyl)-*N*′-ethylcarbodiimide hydrochloride (EDCI) and 1-(4,5-dimethylthiazol-2-yl)-3,5-diphenylformazan (MTT) were purchased from Sigma Aldrich. Acryloyl chloride and citraconic anhydride (Cit) were purchased from Alfa Aesar. IONPs with oleylamine coating were synthesized and characterized by us.[29]

2.2. Synthesis

The synthetic route for the block polymer and IR806 is illustrated in Fig. 1. Briefly, the block polymer mPEG-PCL was synthesized by the ring-opening polymerization of ε-CL and mPEG following the method mentioned in the literature.[30,31] The degree of polymerization of PCL was calculated according to ^{1}H NMR spectrum shown in Fig. 3. G2.0 PAMAM (NH_2-terminated dendrimer)[32] was synthesized following reported methods.[29,33] For the synthesis of IR806 and its functionalized IONPs see ESI.†

Synthesis of the mPEG-PCL-G2.0PAMAM-Cit. For mPEG-PCL-G2.0 PAMAM, an excess amount of acryloyl chloride was first dropped into the anhydrous dichloromethane (DCM) solution of mPEG–PCL–OH (540 mg, 0.074 mmol). The reaction mixture was stirred overnight at 40 °C, and then the intermediates containing –C≡C were synthesized. Finally, Michael reaction was performed between a specified amount of G2.0 PAMAM (240 mg) and the resulting intermediates mentioned above in chloroform; the mixture was stirred at 50 °C for 24 h to complete the reaction. The products were purified, dialyzed and lyophilized for further use.

For mPEG-PCL-G2.0-Cit, briefly, the abovementioned products (250 mg, 0.06 mmol) were added dropwise into 15 mL pyridine and stirred overnight at room temperature. The resulting mixture was poured into a $NaHCO_3$ solution (6%), and purified by dialysis against water for three days (cut-off of 8000–14 000 Da). The final product was obtained with yield of 88% *via* lyophilization. All the synthesized conjugates were characterized by ^{1}H NMR spectroscopy.

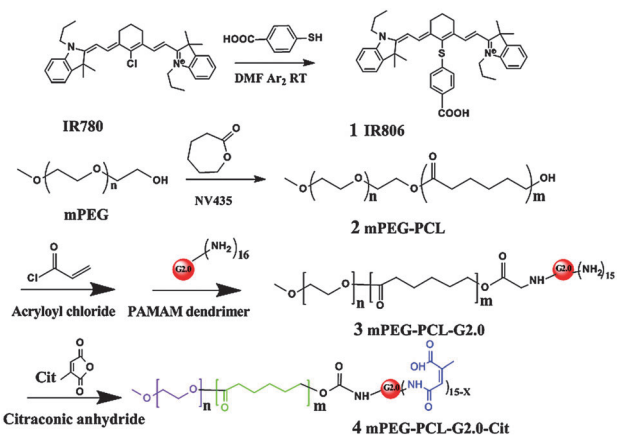

Fig. 1 Schematic illustration of reaction scheme for the synthesis of IR 806 dye and smart polymer of mPEG-PCL-G2.0-Cit.

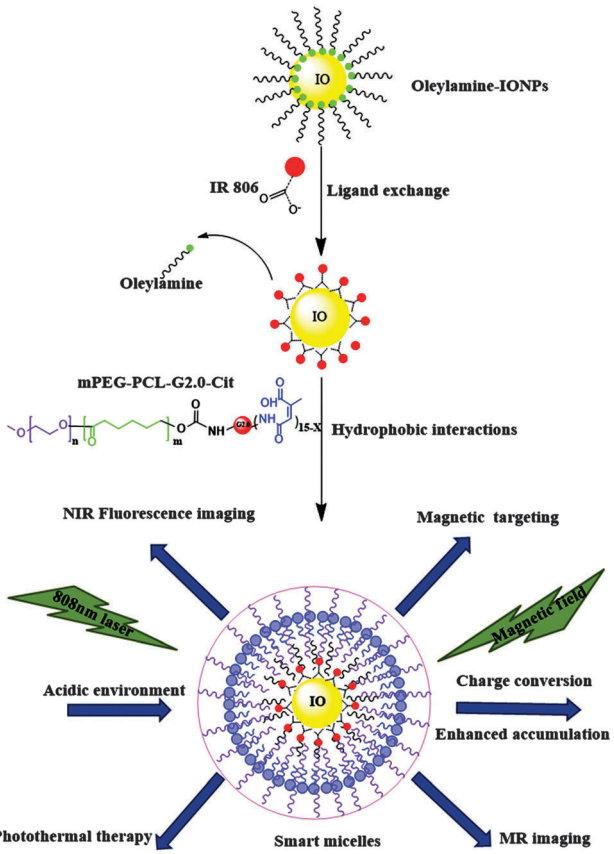

Fig. 2 Schematic diagram presenting direct exchange reactions between the monovalent capping ligand oleylamine and the NIR dye IR806–COOH. The self-assembly process of smart hybrid micelles *via* hydrophobic interaction by functionalized polymer and its biofunctions.

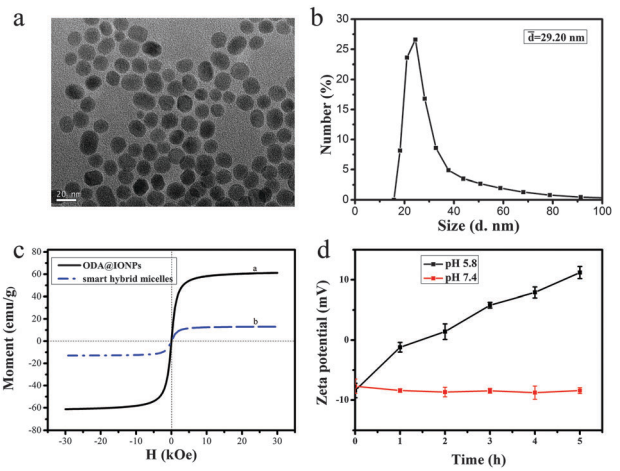

Fig. 3 (a) TEM images of smart hybrid micelles. Scale bar is 20 nm. (b) DLS size of smart hybrid micelles. (c) *M*–*H* curve of oleylamine–IONPs in black and smart hybrid micelles in blue. (d) The zeta potential of smart micelles after incubation at pH 5.8 and 7.4 at 37 °C. The error bars mean standard deviations.

2.3. Preparation of micelles and their charge-conversion behaviour

Briefly, 60 mg mPEG-PCL-G2.0-Cit and 5.0 mg IONPs coated with IR806 were mixed with 2 mL of tetrahydrofuran (THF),

followed by the addition of 2 mL H_2O. The solution was then transferred to a bag and purified using dialysis (cut-off 3500 MW). Subsequently, the as-prepared micelles were purified through centrifugation to remove the excess free polymer and filtered with a 0.22 μm filter. Due to hydrophobic–hydrophobic interactions, this strategy can produce a stable polymer shell on IR806–IONPs. To check the charge-conversion of the hybrid micelles, they were incubated under different pH values and monitored by zeta potential.

Similarly, the non-charge-conversion hybrid micelles and IR806-free IONPs micelles were also prepared and characterized.

2.4. Photostability, temperature stability and photothermal effect

All the prepared micelles were irradiated for 20 min by continuous wave (CW) laser light at 808 nm with 0.25 W cm^{-2}. The absorption and fluorescence spectra were recorded during the laser light irradiation. The hybrid micelles and IONPs or dye-micelles were set at the same concentrations and the temperature of the micelles was measured by a thermocouple thermometer once every minute after irradiation by an 808 nm laser.

2.5. Cellular viability, uptake assay and imaging *in vitro*

Human alveolar adenocarcinoma (A549) and Lewis lung carcinoma (LLC) cells were grown in DMEM supplemented with 10% fetal bovine serum, 100 units per mL penicillin, and 100 μg mL^{-1} streptomycin and cultured in a 5% CO_2 humidified atmosphere at 37 °C. To further confirm the effect of charge-conversion enhanced accumulation of hybrid micelles on the cellular internalization process, the cell uptake of NPs was tested at pH 7.4 and 5.8, and cellular imaging time points were determined by the zeta potential data. A549 cells were incubated in glass bottom cell-culture dishes. After confluent growth for 24 h, the medium was removed and fresh medium containing smart hybrid micelles was added into the corresponding well and incubated at 37 °C; after 3 h and 24 h, the cells were washed three times with PBS. Subsequently, cells were fixed with immunol staining fix solution for 15 min. The dishes were washed three times with PBS and were stained with DAPI, which were then imaged with a modified confocal laser scanning microscope (CLSM, Nikon microscope with a sCMOS camera Hamamatsu ORCA-Flash4.0).

A standard MTT assay was carried out to evaluate the cytotoxicity of smart hybrid micelles against A549 cells with various concentrations, using the cytotoxicity of other micelles as control for 24 h. For PTT killing effect of tumor cells, A549 cells were incubated with different concentrations of hybrid micelles and different power densities of 808 nm laser irradiation at 37 °C. The MTT assay was carried out to evaluate the cell killing effect. To directly observe the PTT efficacy, the hybrid micelles-treated A549 cells were incubated for 24 h. The dishes were washed with PBS three times and the medium was changed with a fresh one followed by irradiation with 808 nm laser light of 0.25, 0.4 and 0.8 W cm^{-2} for 5 min. After an incubation period of 2 h, the treated cells were stained with trypan blue (0.4 wt%) for 3 min and washed with PBS several times.[16]

2.6. *In vivo* efficacy

All the animal studies were carried out in compliance with the animal management protocols. Tumor-bearing mice were produced by the subcutaneous injection of LLC cells in 100 μL PBS in C57 mice (about 20 g, Jilin University Animal Center). The mice models were successfully established for study. As a proof of concept of imaging-guided PTT, we explored the MRI-guided PTT on the tumor-bearing mice, which were randomly divided into four groups, and treated with different preparation conditions. Subsequently, MRI experiments were carried out following our previously reported method.[29,34] For MR imaging, the mice were subjected to an MRI plain scan as control, followed by intravenous injection of the nano-formulations with 200 μL of 2.5 mg mL^{-1}. A distribution study about the intratumoral injection of NPs was also carried out. At the end, after general drug anaesthesia, MR images were obtained at appropriate intervals post-injection with a 1.5T Siemens Avanto MR scanner and an animal coil. All the MRI quantitative analyses were carried out by one radiologist.

For *in vivo* PTT, laser irradiation was focused on the tumor site as determined from MRI. The mice were randomly assigned to four groups for various treatments as follows: (1) group 1 received only injection of PBS; (2) group 2 received injection of PBS with 808 nm light irradiation; (3) group 3 received injection of the smart hybrid micelles only; and (4) group 4 received injection of the smart micelles with 808 nm light irradiation. Mice were irradiated with 808 nm laser light (0.25 W cm^{-2}) for 20 min. All the mice were fed normally and monitored every three days to evaluate the treatment effect. The method for evaluating therapy efficacy was according to a previous study.[35]

2.7. *Ex vivo* histological staining

For histological examination, the organs and tumor tissues of mice were isolated from treated tumor-bearing mice after 14 days, fixed with 10% neutral buffered formalin and embedded in paraffin. Finally, the sliced organs and tumor tissues (8 mm) were stained with Hematoxylin and Eosin (H&E) and images were acquired on a Nikon CS2 microscope.

3 Results and discussion

3.1 Synthesis and characterization of smart hybrid micelles

IR 806 and its functionalized IONPs were confirmed by ^{1}H NMR, FT-IR and absorption spectroscopies (Fig. S1 and S2, ESI†). IR806 was further confirmed by the observation of the characteristic 806 nm absorption peak (Fig. 4a). To confirm the formation of the as-prepared polymers, ^{1}H NMR was used, as shown in Fig. S3 (ESI†). The smart micelles and their IONPs surface coating chemistry are schematically illustrated in Fig. 2. The self-assembly process of smart hybrid micelles was achieved by hydrophobic interactions between IR806-coated IONPs and the functionalized polymer. From the TEM image of smart hybrid micelles shown in Fig. 3a, an average diameter of the micelles was determined to be 20.1 ± 2.6. Dynamic light scattering (DLS) analysis of mPEG-PCL-G2.0-Cit-coated IONPs revealed their size to be around 29.2 nm (Fig. 3b), slightly

higher than the TEM result. This discrepancy may come from the organic portion, which will contract around the IONPs as drying occurs during TEM sample preparation. The DLS size of IONPs and normal hybrid micelles were 9.8 ± 1.2 nm and 24.5 ± 1.4 nm, respectively. Furthermore, the surface morphology of the as-obtained micelles has been analyzed by AFM, which is shown in Fig. S4 (ESI†). All these results confirmed the formation of smart hybrid micelles. The negatively charged micelles with terminal carboxylic groups of Cit led to zeta potentials of the nanoparticles of −8.7 ± 0.15 mV. The charge-reversal behavior of the hybrid micelles was monitored on the basis of the zeta potential after 5 h incubation at pH 7.4 and pH 5.8 at 37 °C. It was found that the charge reversion from negative to positive occurred only in acidic conditions about 2 h later (Fig. 3d); the zeta potential remains negative at pH 7.4, which indicates that the hybrid micelles will be stable at normal physiological pH value.

The saturation magnetization (M_{sat}) of the hybrid micelles is below the value of pure iron oxide because only a fraction of the micelle is magnetic. As can be seen in Fig. 3c, the M_{sat} values of the hybrid NPs were determined to be 12.4 and 65.0 emu g^{-1} for the smart hybrid micelles and IONPs, respectively. In addition, both showed a superparamagnetic property with almost no permanent magnetization and zero coercive fields.

The characteristic absorption spectra of IONPs, IR806 dye-COOH and smart hybrid micelles are shown in Fig. 4a. The absorbance maximum was observed at 806 nm for all the dye-based samples. It is worth noting that phase transfer did not alter the absorption spectrum of IR806. Fig. 4b shows the emission spectra of IR806 under excitation at 750 nm. The major emission peak appears at 833 nm in THF and blueshifts to 831 nm when coated on IONPs and to 820 nm when encapsulated in micelles in water. The differences in emission are presumably due to the electronic state alteration in the dye molecules and the influence of the surrounding environment.

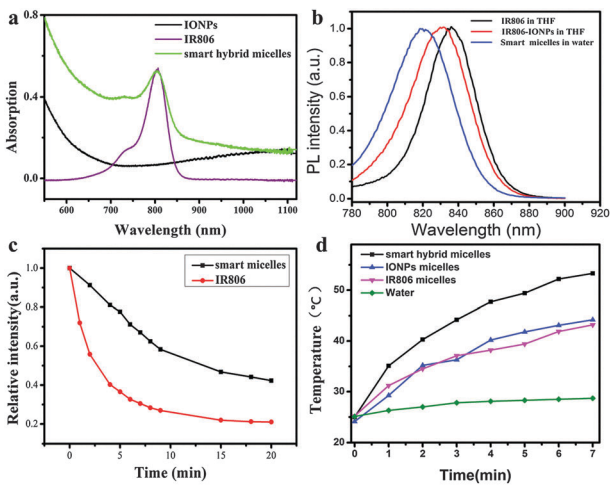

Fig. 4 (a) Absorption spectra of IONPs, IR806 and smart hybrid micelles. (b) NIR photoluminescence spectra of IR806 (in black), IR806-coated IONPs (in red) and smart hybrid micelles (in blue); all the samples were excited at 750 nm. (c) The relative intensity change after irradiation with an 808 nm laser light. (d) Temperature increment in response to irradiation of 808 nm laser light.

Free IR806 dye exhibited serious depletion during 5 min laser irradiation at 808 nm and, surprisingly, the hybrid micelles greatly improved the photostability of the dye, as shown in Fig. 4c. This was mainly because implanting dye-coated IONPs inside a hydrophobic core of micelles could efficiently form shield protection from the decomposition upon irradiation and decrease the non-radiative processes, thus endowing hybrid micelles with considerably better photostability than the corresponding free IR806 dye.

The photothermal effects of all the samples were evaluated *in vitro* under 808 nm light irradiation using a thermocouple needle. Compared with water, hybrid micelles containing IONPs and dye-micelles were more efficient than individual IONPs and IR806 dye-micelles in inducing a temperature increase with the same exposure time. When the water temperature was increased by 4 °C, the temperature of IONPs and dye-micelles increased by 17 °C and 18 °C, respectively (Fig. 4d), while for the smart hybrid micelles, it increased by 28 °C. Such a temperature increase of the NPs could lead to an irreversible damage to tumor cells.

3.2 Cellular experiments

The delivery efficiency of the smart hybrid micelles on A549 cells was examined by a modified CLSM. The cell images after incubation at pH 5.8 and pH 7.4 for 3 and 24 h are shown in Fig. 5. After 3 h incubation, the smart hybrid micelles incubated at pH 5.8 had considerably higher fluorescence intensity than those at pH 7.4. After 24 h incubation, the fluorescence intensity increased even further. This was mainly because of Cit forming β-carboxylic-acid amides in hybrid micelles, which caused the charge-conversion from negative to positive upon exposure to the acidic tumor environment. Once the smart materials were exposed to an acidic environment, including extracellular or acidic organelles in the tumor, the smart platform would hydrolyze and restore the original amines, which effectively enhanced the accumulation by electrostatic absorptive endocytosis.

Following cellular internalization, another key issue is whether the smart hybrid micelles can be efficiently scalded to death with an 808 nm laser light. In Fig. 6, the relative viabilities of A549 lung cancer cells were evaluated by standard MTT assay after incubation with the as-obtained micelles at various concentrations. It can be seen that there was no significant toxicity observed for all the NPs used with the A549 cell lines even with concentration as high as 500 μg mL^{-1}, indicating the excellent biocompatibility of the NPs. The cytotoxicity of micelles had also been evaluated with normal cells (mouse microglia cell, BV2, Fig. S5, ESI†). The MTT results are consistent with the A549 cells. On the other hand, the viability of A549 cells decreased dramatically with the increase of the 808 nm light irradiation power, as shown in Fig. 7b, demonstrating a great PTT killing effect of tumor cells. Direct observation of the PTT efficacy, through a trypan blue stained method, was carried out on the treated cells in Fig. S6 (ESI†). Dead cells were trypan blue-stained and live cells were non-stained. Before 808 nm

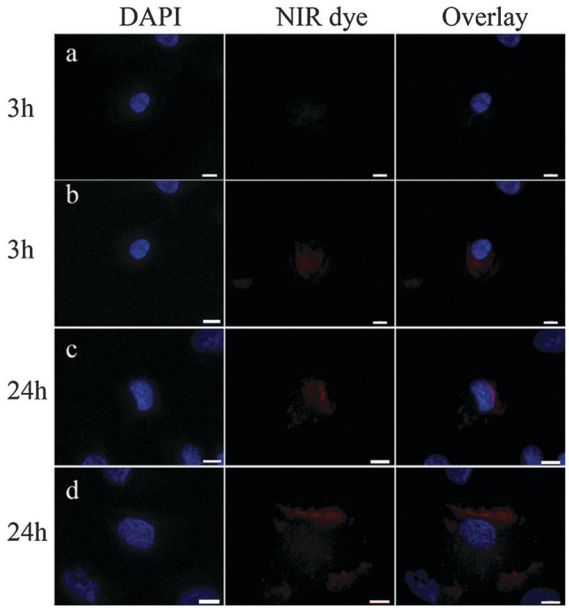

Fig. 5 Dark field microscope images of intracellular micelles with smart capping ligands of citraconic amide. For each panel, the images from left to right show cell nuclei stained by DAPI (blue), NIR dye fluorescence in cells (red), and overlays of the two images. The scale bars are 10 μm in all the images. (a) 3 h incubation, pH 7.4; (b) 3 h incubation, pH 5.8; (c) 24 h incubation, pH 7.4; (d) 24 h incubation, pH 5.8.

laser irradiation, all the treated cells were alive. Once 808 nm laser light was irradiated onto the IR806–IONPs based micelles, large numbers of cells were killed by the thermal effect arising from the hybrid micelles.

3.3 *In vivo* MRI

We explored the charge-conversion manner of the prepared nanoplatform as an MRI contrast agent for tumor imaging. Simultaneously, the normal IONPs micelles and PBS group were used as control. The T_2-weighted MRI for all the mice was conducted at 3 h and 24 h post-injection relative to pre-injection, as shown in Fig. 7. Negative enhancing effect of IONPs (namely, darkening of T_2 imaging) accumulation was observed compared with groups injected with PBS intravenously (Fig. 7a). The non-charge-reversal micelles (normal hybrid micelles) show only a slight

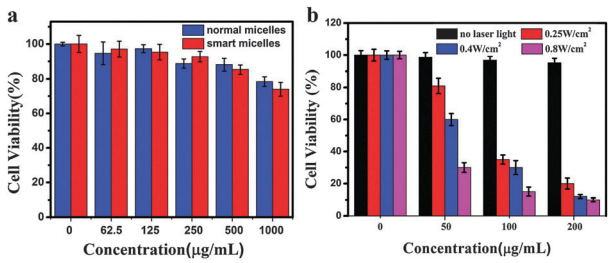

Fig. 6 (a) *In vitro* cell viability of A549 cells incubated for 24 h with different concentrations of smart hybrid micelles. Cell viability assays were carried out using MTT method. (b) The photo-cytotoxicity of smart hybrid micelles in A549 cells with or without 0.25 W cm^{-2} 808 nm laser irradiation for 5 min. Data is shown as mean ± SD, $n = 3$, $P < 0.05$.

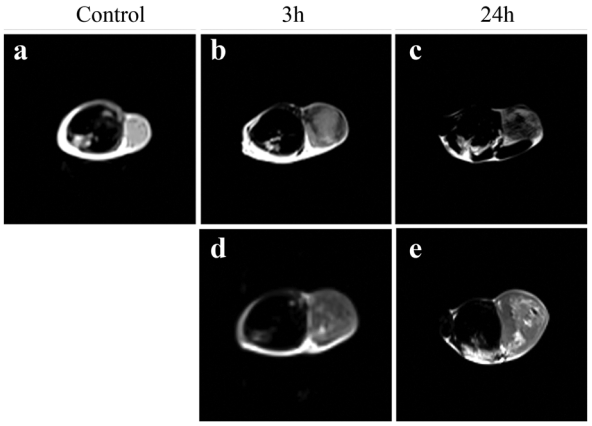

Fig. 7 *In vivo* T_2-weighted MR imaging analysis of C57 mice bearing LLC tumor after tail vein injection and intratumoral injection of NPs. Intravenous injection of (a) PBS, (b) smart micelles post-injection 3 h intravenous injection, (c) smart micelles post-injection of 24 h, (d) normal micelles post-injection of 3 h, and (e) normal micelles post-injection of 24 h.

enhancement after 3 h (Fig. 7d), while the smart charge-conversion NPS represent a better MR contrast in Fig. 7b, which is consistent with the cell results. However, after 24 h, the normal hybrid micelles without Cit-modified polymer also demonstrated contrast enhancement Fig. 7e. This can be explained by the enhanced permeability and retention (EPR) effect caused by normal hybrid micelles accumulation in the tumor site, indicating that targeting and the EPR effect are both important in drug delivery.[36–38] Guided by this, we took the point time of 24 h post-injection for PTT treatment. Our results indicated that the smart hybrid micelles may be suitable for imaging-guided therapy.

3.4 *In vivo* therapeutic efficacy of PTT

To better evaluate the PTT effect on tumors, we randomly divided tumor-bearing mice into four groups treated with different preparations followed by PTT triggered by 808 nm light at 0.25 W cm^{-2}. The growth rate of tumors was monitored every three days to evaluate the treatment effect. Based on the results of MR imaging, the PTT was carried out after 24 h post-injection. First, we evaluated the thermal effect of nanoparticles *in vivo*. After 2 min of 808 nm laser irradiation, the mice treated with normal and smart nano-complexes had a temperature of 44.7 and 46.3 °C, respectively. However, the control group treated with PBS under the same conditions caused a maximum temperature increase of 4.5 °C, which is insufficient for killing the tumor. Representative photos of tumor-bearing mice before and after various treatments were obtained after 14 days, as shown in Fig. S7 (ESI†). Three days later, the tumor-bearing mice treated with smart NPs showed slight skin damage at the irradiation site. This significant therapeutic effect was not observed in the control groups of PBS and 808 nm light only, which further confirmed the well known thermal effect of organic–inorganic hybrid materials. After PTT, the experimental groups showed significant tumor inhibition, in contrast to the control groups where the mice were treated with PBS and NPs without 808 nm light irradiation that did not show any therapeutic effect.

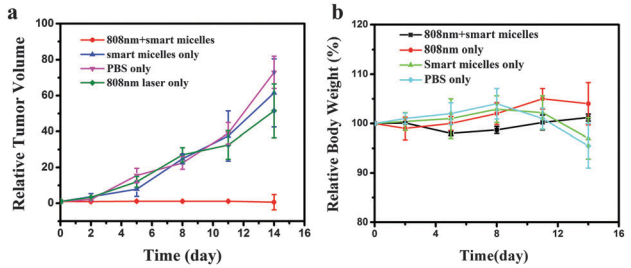

Fig. 8 *In vivo* therapeutic efficacy of smart hybrid micelles for photothermal therapy. 24 h after the tail vein was injected, the mice were irradiated by 808 nm light with a power density of 0.25 W cm^{-2}. (a) Tumor growth curves of different groups of mice after various treatments and (b) body weight in different groups with treatment. n = 6 per group; $p < 0.05$; error bars were based on standard error of mean.

Subsequently, we monitored the tumor volume and body weight changes until 14 days post-injection, as shown in Fig. 8. The relative tumor volumes were normalized to their initial sizes. The tumors of all the control groups grew rapidly and even the size exhibited more than 52-fold increase of average tumor volumes compared to their original volumes (102.8 ± 18.7 mm^3). This indicated that photo-irradiation itself and only injection of PBS or hybrid micelles have a negligible influence on tumor growth. Surprisingly, tumors treated with the smart hybrid micelles + 808 nm laser group showed significant tumor inhibition or even complete ablation of the tumor. The changes of body weight can also reflect the health condition of the treated mice, which further confirmed the biocompatibility of the micelles, as shown in Fig. 8b. With the tumor volume increasing, the body weight of mice in the control group began to decrease from 8-day treatment, which indicated that the living quality of the mice was affected by the tumor burden. These results illustrate the potential of the smart hybrid micelles as a tumor-microenvironment sensitive and imaging-guided therapeutic platform of tumor.

The histological analyses on tumor and major organs were carried out in different treatment groups after 14 days of post-treatment. We can find no pathological changes in the heart, liver, spleen, lung, or kidney, as shown in Fig. 9. Compared with the control groups, we found that myocardial cells were arranged orderly; no congestion, ischemia, and no inflammatory cell infiltration were observed; the structure of hepatic lobules, portal vein, and bile duct were also normal; by comparing the spleens, there was no significant difference between the control group and the treatment group. The structure of alveolae was normal and alveolar epithelial cells showed no necrosis; finally, the number and the structure of glomerular, renal tubule were the same as normal. The results suggested the biosafety of the smart micelles as an efficient PTT agent.

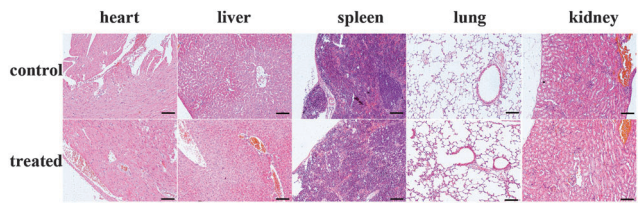

Fig. 9 H&E-stained histological images of five organ tissues (heart, liver, spleen, lung and kidney) from the mice treated with smart hybrid micelles. The scale bar is 100 μm.

4 Conclusions

In summary, a smart photothermal nanoplatform with high efficacy and biosafety has been successfully constructed for imaging-guided PTT. A pH-sensitive charge-conversion strategy was introduced to the nanoplatform, which improved the uptake efficiency. We demonstrated the effective PTT on mice under the combined photothermal effect of NIR dye and IONPs, driven by low power density of 808 nm laser light at 0.25 W cm^{-2}, which was an obvious optimization of currently applied power density for single PTT agent. Our study highlights the potential of the nano-agent for precision medicine.

Acknowledgements

This study was financially supported by the NSF of China (11174277, 11374297, 61275202, 21304084, 11474278 and 51372096), Joint research program between CAS of China and KNAW of the Netherlands, the IOP program of the Netherlands, EU COST Action CM1403, and John van Geuns foundation. We are grateful to Dr Dongmei Yan and Qihui Liu (Basic Medical Sciences, Jilin University.) for establishing the tumor model.

References

1 X. Cai, X. Jia, W. Gao, K. Zhang, M. Ma, S. Wang, Y. Zheng, J. Shi and H. Chen, *Adv. Funct. Mater.*, 2015, **25**, 2520–2529.
2 X. Song, R. Zhang, C. Liang, Q. Chen, H. Gong and Z. Liu, *Biomaterials*, 2015, **57**, 84–92.
3 V. Shanmugam, S. Selvakumar and C. S. Yeh, *Chem. Soc. Rev.*, 2014, **43**, 6254–6287.
4 D. Shi, M. E. Sadat, A. W. Dunn and D. B. Mast, *Nanoscale*, 2015, **7**, 8209–8232.
5 P. Huang, J. Lin, X. S. Wang, Z. Wang, C. L. Zhang, M. He, K. Wang, F. Chen, Z. M. Li, G. X. Shen, D. X. Cui and X. Y. Chen, *Adv. Mater.*, 2012, **24**, 5104–5110.
6 Y. L. Zhao and R. J. Zhang, *J. Phys. Chem. A*, 2007, **111**, 7189–7193.
7 Y. Wang, H. Wang, D. Liu, S. Song, X. Wang and H. Zhang, *Biomaterials*, 2013, **34**, 7715–7724.
8 M. Guo, H. Mao, Y. Li, A. Zhu, H. He, H. Yang, Y. Wang, X. Tian, C. Ge, Q. Peng, X. Wang, X. Yang, X. Chen, G. Liu and H. Chen, *Biomaterials*, 2014, **35**, 4656–4666.
9 J. Croissant, M. Maynadier, O. Mongin, V. Hugues, M. Blanchard-Desce, A. Chaix, X. Cattoen, M. W. C. Man, A. Gallud, M. Gary-Bobo, M. Garcia, L. Raehm and J. O. Durand, *Small*, 2015, **11**, 295–299.
10 J. Croissant, D. Salles, M. Maynadier, O. Mongin, V. Hugues, M. Banchard-Desce, X. Cattoen, M. W. C. Man, A. Gallud,

M. Garcia, M. Gary-Bobo, L. Raehm and J. O. Durand, *Chem. Mater.*, 2014, **26**, 7214–7220.
11 T. J. Manning, L. Taylor, J. Purcell and K. Olsen, *Carbon*, 2003, **41**, 2813–2818.
12 T. Yanagi, H. Kajiya, M. Kawaguchi, H. Kido and T. Fukushima, *J. Biomater. Appl.*, 2015, **29**, 1109–1118.
13 Y. C. Chuang, C. J. Lin, S. F. Lo, J. L. Wang, S. C. Tzou, S. S. Yuan and Y. M. Wang, *Biomaterials*, 2014, **35**, 4678–4687.
14 S. H. Seo, B. M. Kim, A. Joe, H. W. Han, X. Chen, Z. Cheng and E. S. Jang, *Biomaterials*, 2014, **35**, 3309–3318.
15 M. Manikandan, N. Hasan and H. F. Wu, *Biomaterials*, 2013, **34**, 5833–5842.
16 C. Yue, P. Liu, M. Zheng, P. Zhao, Y. Wang, Y. Ma and L. Cai, *Biomaterials*, 2013, **34**, 6853–6861.
17 H. Yang, H. J. Mao, Z. H. Wan, A. J. Zhu, M. Guo, Y. L. Li, X. M. Li, J. L. Wan, X. L. Yang, X. T. Shuai and H. B. Chen, *Biomaterials*, 2013, **34**, 9124–9133.
18 L. Wu, S. T. Fang, S. Shi, J. Z. Deng, B. Liu and L. T. Cai, *Biomacromolecules*, 2013, **14**, 3027–3033.
19 K. C. Barick, S. Singh, D. Bahadur, M. A. Lawande, D. P. Patkar and P. A. Hassan, *J. Colloid Interface Sci.*, 2014, **418**, 120–125.
20 Y. B. Li, W. Lu, Q. A. Huang, M. A. Huang, C. Li and W. Chen, *Nanomedicine*, 2010, **5**, 1161–1171.
21 X. Zhang, X. W. Xu, T. T. Li, M. Lin, X. Y. Lin, H. Zhang, H. C. Sun and B. Yang, *ACS Appl. Mater. Interfaces*, 2014, **6**, 14552–14561.
22 X. Yang, C. Shi, R. Tong, W. Qian, H. E. Zhau, R. Wang, G. Zhu, J. Cheng, V. W. Yang, T. Cheng, M. Henary, L. Strekowski and L. W. Chung, *Clin. Cancer Res.*, 2010, **16**, 2833–2844.
23 S. Luo, E. Zhang, Y. Su, T. Cheng and C. Shi, *Biomaterials*, 2011, **32**, 7127–7138.
24 S. Shen, S. Wang, R. Zheng, X. Zhu, X. Jiang, D. Fu and W. Yang, *Biomaterials*, 2015, **39**, 67–74.
25 L. Nie and X. Chen, *Chem. Soc. Rev.*, 2014, **43**, 7132–7170.
26 E. Zhang, S. Luo, X. Tan and C. Shi, *Biomaterials*, 2014, **35**, 771–778.
27 G. Shan, R. Weissleder and S. A. Hilderbrand, *Theranostics*, 2013, **3**, 267–274.
28 X. Song, H. Gong, T. Liu, L. Cheng, C. Wang, X. Sun, C. Liang and Z. Liu, *Small*, 2014, **10**, 4362–4370.
29 Y. L. Chang, X. L. Meng, Y. L. Zhao, K. Li, B. Zhao, M. Zhu, Y. P. Li, X. S. Chen and J. Y. Wang, *J. Colloid Interface Sci.*, 2011, **363**, 403–409.
30 S. W. Wang, Z. Bao, P. Ai, M. Zhu, W. Wang, S. P. ZhongPeng, L. N. Ma and L. P. YaPeng, *Sci. China, Ser. B: Chem.*, 2009, **52**, 2336–2341.
31 F. Ahmed and D. E. Discher, *J. Controlled Release*, 2004, **96**, 37–53.
32 Y. L. Zhao, Y. T. Song, W. Jiang, B. Zhang, Y. P. Li, K. Sha, S. W. Wang, L. Chen, L. Ma and J. Y. Wang, *J. Appl. Polym. Sci.*, 2008, **109**, 1039–1047.
33 D. A. Tomalia, A. M. Naylor and W. A. Goddard III, *Angew. Chem., Int. Ed.*, 1990, **29**, 138–175.
34 Y. L. Chang, N. A. Liu, L. Chen, X. L. Meng, Y. J. Liu, Y. P. Li and J. Y. Wang, *J. Mater. Chem.*, 2012, **22**, 9594–9601.
35 L. Xia, X. G. Kong, X. M. Liu, L. P. Tu, Y. L. Zhang, Y. L. Chang, K. Liu, D. Z. Shen, H. Y. Zhao and H. Zhang, *Biomaterials*, 2014, **35**, 4146–4156.
36 H. Lee, E. Lee, D. K. Kim, N. K. Jang, Y. Y. Jeong and S. Jon, *J. Am. Chem. Soc.*, 2006, **128**, 7383–7389.
37 H. Maeda and Y. Matsumura, *Adv. Drug Delivery Rev.*, 2011, **63**, 129–130.
38 H. Maeda, J. Wu, T. Sawa, Y. Matsumura and K. Hori, *J. Controlled Release*, 2000, **65**, 271–284.